# Transmission of sound beams through the interface between two fluids

Rolf J. Korneliussen,[a] Halvor Hobaek, and Gunnar Lien
*Department of Physics, University of Bergen, Allégt. 55, N-5007 Bergen, Norway*

(Received 14 December 1990; accepted for publication 20 February 1991)

In this article, results from an experiment on the transmission of a sound beam at and above critical incidence onto an interface between two fluids, which are chosen to simulate a water/sand interface, are presented. The incident beam is produced from a parametric array that is arranged to intersect the interface either within the absorption limit of the primary waves, or far outside the same, with the aim to discriminate whether linear or nonlinear processes are responsible for the transmission. Postcritical transmission is found to be basically a linear process, and is observed out to about 10° above the angle of critical incidence. Interference between the transmitted field and evanescent waves is observed just beneath the interface. The asymptotic axis of the main penetrating beam is investigated with respect to refraction angle and beam displacement. The field structure becomes markedly different if the primary waves are intersected by the interface, the main difference being the presence of a strong "underlobe" that has no direct counterpart in the incident field as measured in free field. This change in field structure is attributed to nonlinear effects, the candidates of which are discussed in detail. The most likely of these are the effects of primary beam truncation suggested by D. J. Wingham ["A theoretical study of the penetration of a water sediment interface by a parametric beam," J. Acoust. Soc. Am. **76**, 1192–1200 (1984)] and nonlinearity of the boundary conditions at the interface where the primary beams are intersected.

PACS numbers: 43.30.Ma, 43.30.Qd

## INTRODUCTION

The present article is an experimental study of the transmitted field of a sound beam intersecting an interface between two homogeneous fluid layers above critical incidence. The incident beam is produced by a parametric array. To discriminate between linear and nonlinear contributions to the transmitted field, the parametric array was modeled to (a) taper the primary waves by absorption such that they could be regarded as nonexistent at the interface, and (b) let the primary waves reach the interface only moderately attenuated. In both cases, a transmitted field was observed. However, the structure of the field is different in the two cases. The objective of the experiment is to provide experimental data with no bias in any specific theory.

The first experimental results on this problem were published by Muir *et al.*[1,2] In a model experiment on transmission from water to sand with both a narrow parametrically generated sound beam and a wider conventional sound beam, they observed several unexpected features with the parametric array when the angle of incidence was near or greater than the critical angle of incidence. At postcritical angle of incidence, where plane-wave theory predicts total reflection (for lossless media), energy was still found to be transmitted into the bottom. They also observed that near critical incidence, the beam seemed to be displaced along the interface before entering the sediment. However, when the sound was generated by a conventional source, none of these effects were observed.

These results triggered a lot of interest. Horton[3] analyzed the effect of absorption on the evanescent wave field below the interface. Berktay and Moustafa[4] obtained experimental results with a conventional sound source that indicate that postcritical transmission is not necessarily related only to parametric arrays. Naze Tjøtta and Tjøtta[5] presented an extensive analysis based on substituting the incident beam with a source distribution on the interface. They concluded that postcritical transmission is a linear process that requires that the size of the spot must not be large compared to the wavelength. Here the "spot" is the area on the interface insonified by the incident wave field.

Wingham[6] suggested a different explanation based on the nonlinear nature of the parametric array assuming that the primary waves are truncated by the interface. In his own words, "The field is found to be due to two source apertures, one consistent with the transducer, the second with the truncation." This is, however, hardly a useful description of the physics of the model, but rather an interpretation of the mathematical expression obtained. As we understand this model, the essential difference from ordinary parametric arrays lies in the oblique truncation volume, where the effective aperture of the virtual sources of equal phase becomes tapered as range increases. This implies that a less directive field is radiated from this volume than would be the case in free field. This paper was followed with a clever experiment largely supporting the theory, Wingham *et al.*,[7] but unfortunately neither the theoretical nor the experimental results were published in a form that made comparison to other results easy.

Jensen and Schmidt[8] applied the SAFARI model[9] to the

[a] Present address: Institute of Marine Research, P.O. Box 1870, N-5011 Bergen, Norway.

 0001-4966/91/062696-15$00.80  

problem with a two-dimensional numerical solution where the beam is formed by a vertical focused array of (linear) elementary line sources such that the focal region coincides with the interface. Their results agree with those of Ref. 5 for the transmitted field, within reasonable limits set by different conditions in the two models.

In Ref. 10 Naze Tjøtta *et al.* present numerical results from a two-dimensional model where the source is modeled as a horizontal source distribution at a distance from the interface. They focus attention to the direction and displacement of the beam axis, which is shown to depend on both absorption and source height above the interface, in addition to source width and incidence angle. (The definition of beam axis will be discussed in Secs. I and III.) Similar results are presented by Salvesen *et al.*[11] where the position of the beam axis is determined without explicit computation of the sound field.

Recent experimental results are reported by Williams *et al.*[12] They apply two different parametric arrays to investigate the transmitted field where the primary waves either reach the interface relatively unattenuated or are absorbed before reaching the interface. The second medium is sand, and the field is mapped with buried hydrophones by moving the sound source horizontally—A technique that also was used by Wingham *et al.* They compare their results with numerical results from the SAFARI model, and claim excellent agreement, concluding that postcritical transmission is a linear process. In spite of this, their results are presented in a form that is difficult to apply for comparison to other experiments and theory.

Thus we feel that there is still a need for experimental results to clarify the details of the transmitted field at postcritical incidence. We have chosen a similar procedure to Williams *et al.* by using two different parametric arrays in order to discriminate between linear and nonlinear effects. In contrast to their large scale experiment, our measurements are taken with a scaled model experiment at high frequencies, making complete control of the experimental parameters possible. The results show a high degree of structure in the transmitted field, which is analyzed, and an explanation is attempted. Whenever possible the results are compared to theory.

In Sec. I, the experimental conditions are described. Section II describes the results obtained with the two parametric arrays, which is analyzed and discussed in Sec. III. Here, we also discuss the linear and nonlinear mechanisms that may contribute to postcritical transmission. The article ends with a summary and conclusions. A brief characterization of the parametric arrays used is given in the Appendix.

## I. EXPERIMENT

Since sediments like sand and clay are poor carriers of transverse waves, reflection and transmission can be studied with two immiscible liquids instead of water and sand. This greatly simplifies the practical implementation of the experiment, because it is possible to move the hydrophone continuously on both sides of the interface. Another advantage by using two liquids is that the interface is automatically plane and horizontal. It is, however, not possible to obtain the same absorption coefficients as in sediments, where absorption is proportional to the frequency (approximately), while absorption in (Newtonian) liquids is proportional to the squared frequency. "Lamp oil" (a highly refined kerosene) was used as the upper liquid and fresh water as the lower. The sound speeds of the two liquids produce a critical angle of $62.4 \pm 0.4°$, which is not far from that of a water/sand interface. The uncertainty is caused by variation of the temperature, which was difficult to keep completely constant during the runs. Thus the temperature was $25.2 \pm 0.75$ °C. The sound speed in water was measured to $c_2 = 1499.5$ m/s at 25.2 °C. Data for sound speed, density, and the nonlinearity parameter ($B/A$) in the lamp oil was kindly provided by Eric Carr Everbach of Yale University, and is presented in Table I. The absorption coefficient $\alpha$ was determined to $\alpha/f^2 = 2.9 \times 10^{-13}$ (s$^2$/m) within 10%, where $f$ is frequency.

TABLE I. Sound speed, density, and nonlinearity parameter ($B/A$) in "lamp oil" at different temperatures.

| Temperature °C | Sound speed m/s | Density kg/m$^3$ | $B/A$ |
|---|---|---|---|
| 20 | 1347.8 | 803.2 | 10.7 |
| 25 | 1328.9 | 799.7 | 10.9 |
| 30 | 1310.5 | 796.5 | ··· |
| 35 | 1284.2 | 792.4 | ··· |

Naze Tjøtta and Tjøtta's theory[5] is valid for $ka \gg 1$, where the wave number $k = 2\pi f/c_2$ is referred to the lower medium, and $a$ is a characteristic measure of the spot size, for example the beam radius at the interface. This condition is assumed to be fulfilled if $ka \geqslant 6$. The smaller the value of $ka$, the steeper the beam is expected to penetrate into the sediment. In their experiment, Muir *et al.*[2] used $ka \approx 20$ on the interface. For this reason $ka$ in the present experiment was chosen to lie in the range 6–20.

A small spot size is more easily obtained by using a parametric acoustic array than by a conventional sound source. In order to investigate whether transmission at postcritical angles is mainly of linear or nonlinear nature, we decided to use two different parametric arrays. The first one of these has a circular primary source of radius 15.1 mm and a resonance frequency at 4.25 MHz. This yields an arraylength $L_A$ of approximately 9.5 cm in lamp oil, where the array length is defined as $L_A = (\alpha_a + \alpha_b - \alpha_-)^{-1}$, and $\alpha_a$, $\alpha_b$, and $\alpha_-$ are the absorption coefficients at the two primary frequencies and the difference frequency, respectively. The second array has a primary source of radius 12.5 mm and primary frequencies centered about 1.77 MHz, which gives an arraylength of 45 cm in lamp oil. For both sources, the requirement $6 < ka < 20$ restricts the difference frequency $f_-$ to the range 100–300 kHz. In this experiment, 250 kHz was used for most of the runs. Additional parameters for the arrays are summarized in the Appendix.

In a parametric array, the nonlinear interaction takes place mainly within one arraylength from the primary source, and can be neglected at distances greater than about

three arraylengths, where only 5% is left of the initial primary energy. This distance should not be confused with the near-field length of the parametric array, which is very much greater. This can be defined as the range where the directivity pattern becomes range independent. Moffett and Mellen[13] approximate this near-field length with $R_0 f_0/f_-$, where $R_0 = k_0 a^2/2$ is the primary Rayleigh distance, (subscript 0 refers to the mean primary frequency). This is, however, a simplification of the actual situation,[14] which depends on, among other factors, in which of the parameter regions the array belongs (see Appendix).

The tank used in this experiment allowed positioning of the source relative to the interface such that the 4-MHz array produced a small spot at the interface, while the primary waves were almost completely damped away, whereas the 2-MHz array produced a spot of about half this size, but with much energy still present in the primary waves at the interface. The spot size is determined by the − 3-dB radius of the beam. If the primary waves may be regarded as almost totally reflected at postcritical incidence, the interaction region is effectively truncated by the interface, and the conditions of the model in Ref. 6 should apply. These two parametric arrays should therefore adequately distinguish between the two types of models: If the 4-MHz array at intersection ranges $L > 3L_A$ produces postcritical transmission the effect is of linear nature. On the other hand, if only the 2-MHz array produces postcritical transmission while the 4-MHz array does not, we may imply that the effect is of nonlinear origin only. It has not been possible to adjust the experimental parameters to exactly correspond to any of the published theoretical results.[5,6,8,10]

The hydrophone used in this experiment was a Brüel & Kjaer 8103. Although its frequency response is not constant above 140 kHz, it is sensitive at even higher frequencies, and only relative measurements of the sound pressure at a single frequency are needed. It's sensitive element is a ceramic tube of diameter 7 mm, which is only slightly greater than the wavelength in water at 250 kHz. Thus any uncertainty in position due to the finite size of the hydrophone is regarded negligible.

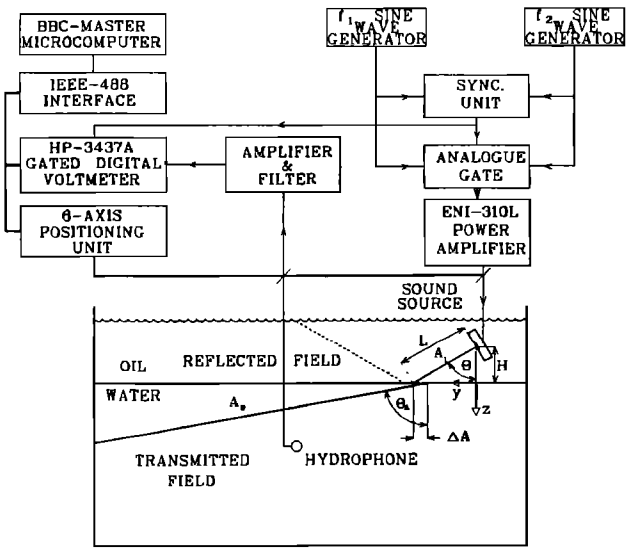


FIG. 1. Experimental configuration and geometry. The upper fluid in the tank is oil, the lower tap water.

Figure 1 describes the experimental configuration and defines the coordinates used in presenting the data. The origin is taken at the vertical projection of the source center onto the interface. The $z$ axis (depth) is vertically downward, and the $y$ axis (horizontal range) is along the interface centrally in the tank. The acoustic axis $A_1$ in the upper medium is defined as the line perpendicular to the source face through its center, and coincides with the direction of maximum sound intensity of difference frequency sound. Let $L$ be the distance along the acoustic axis from the center of the source to the interface. The incidence angle is the angle between $A_1$ and the $z$ axis.

In the lower medium the beam axis, i.e., the acoustic axis $A_2$ is harder to define. We have chosen to locate the pressure amplitude maximum as a function of range using pressure level plots by tracing the path of least steep descent. The resulting curve approaches asymptotically a straight line, which we define as the acoustic axis. Note that this approach differs from those used in Refs. 5 and 10. This difference is discussed in Sec. III.

The angle of refraction, $\theta_A$, is defined as the angle between $A_2$ and the $z$ axis. $\Delta A$ is the distance between the intersection of $A_1$ and $A_2$ with the interface, and is defined as positive if $A_1$ intersects closer to the origin than $A_2$.

Figure 1 also shows a block diagram of the electronics equipment. The sound was transmitted as intermittent bursts, in order to avoid reflections from the walls and from the suspension of the hydrophone. The sound field measured with the hydrophone was sampled with a HP 3437A System Voltmeter, after amplification and filtering. Continuous wave conditions were obtained artificially by sampling the signal in the stable region after the transients had died out. Only one sample was taken for each burst, so the amplitude had to be determined by sampling a number of successive bursts at slightly increasing delays. All measurements of pressure amplitude were done at the same period, approximately in the middle of the burst. Moreover, at each delay an average over ten samples was made to reduce noise.

The position and orientation of both the source and the hydrophone were remotely controlled by a microcomputer, which also controlled the data recording. The sound field in the lower fluid (water) was sampled by moving the hydrophone in a plane with steps of about 5 mm, for a total of 120 steps horizontally, and 40 steps vertically. The time needed for recording the field for one set of parameters was about 36 h.

## II. RESULTS

### A. 4-MHz array

The primary source was positioned to an accuracy in height of $\Delta H = 0.5$ mm, and of angle $\Delta\theta = 0.1°$. The accuracy of the hydrophone position was: $\Delta x = 0.5$ mm, $\Delta y = 0.6$ mm and $\Delta z = 1$ mm. The hydrophone was moved horizontally away from the source, lowered to the next depth at the

end of the trace, and moved horizontally back again until the carriage reached a stopping block, fixed at a suitable distance from the source. Thus horizontal position is reset at every other trace, and any accumulating error in $y$ position is reduced to maximally $\pm 1$ mm at the end of every second horizontal trace.

Figure 2 shows a contour map of a vertical section of the incident field as measured in oil with the acoustic axis oriented horizontally. The location of the interface for some of the cases investigated below is indicated as straight lines. The primary source is indicated (the square bracket looking item) to the left of the frame, which covers only the range 44–644 mm and about 100 mm to each side of the axis. In this map, as in most of the subsequent ones, depth is scaled a factor of 2 with respect to range. The contours are separated by 3 dB and are normalized to 0 dB at the maximum pressure amplitude within the frame. The contours below $-39$ dB are suppressed. None of the contour plots presented here has been subject to data smoothing.

This map demonstrates clearly the typical pattern of a parametric array where the difference frequency amplitude is generated in the medium by the interacting primary waves. For example, in this case, the maximum pressure amplitude on the axis is reached at about $2L_A$ from the primary source.

A different presentation of the incident beam is the amplitude profile as it would appear along the interface. This is shown in Fig. 3 for the case $L = 5L_A$, $\theta = 69°$. The profile is extracted along the corresponding straight line in Fig. 2 from the same data set. The reference amplitude is the same as in Fig. 2. This profile differs from the profile taken at a right angle to the axis, partly because the range from the primary source varies strongly, causing an amplification of the field at closer horizontal ranges over that at longer ranges, but also because as horizontal range increases the incidence angle of the corresponding ray increases more and more slowly. In fact, because of the high directivity of the beam the latter effect dominates. Thus a symmetric incident beam will result in an asymmetric profile along the interface at these high incidence angles. The horizontal range in Fig. 3 is referred to the projection of the primary source center onto the interface, and corresponds to $y$ in Fig. 1. Observe that at $-35$ dB ( $-32$ dB referred to the profile maximum), there is a small hump in the profile. This may indicate the presence of a rudimentary sidelobe in the incident field. This has earlier been observed in parametric arrays of this type,[15] where absorption terminates the nonlinear interaction inside the near field of the primary waves.

Measurements of the transmitted field were taken for

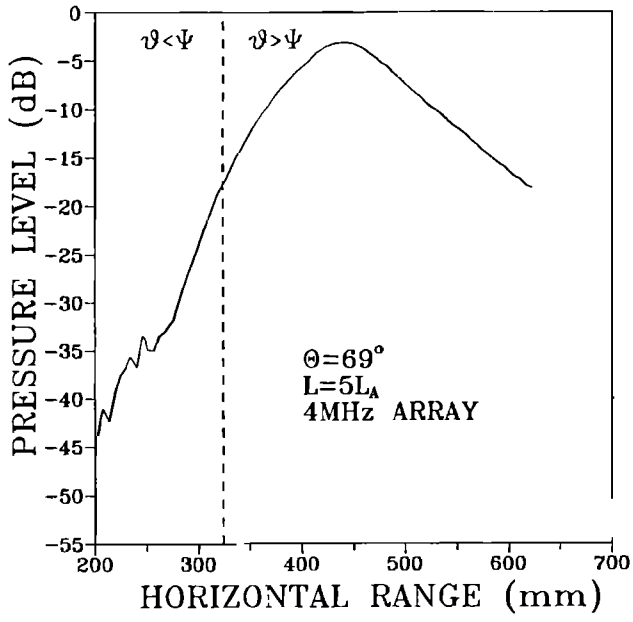


FIG. 3. Profile of incident field along the interface for the 4-MHz array. Ranges to the right of the vertical dotted line correspond to incidence angles greater than the critical angle, denoted Ψ in this figure.

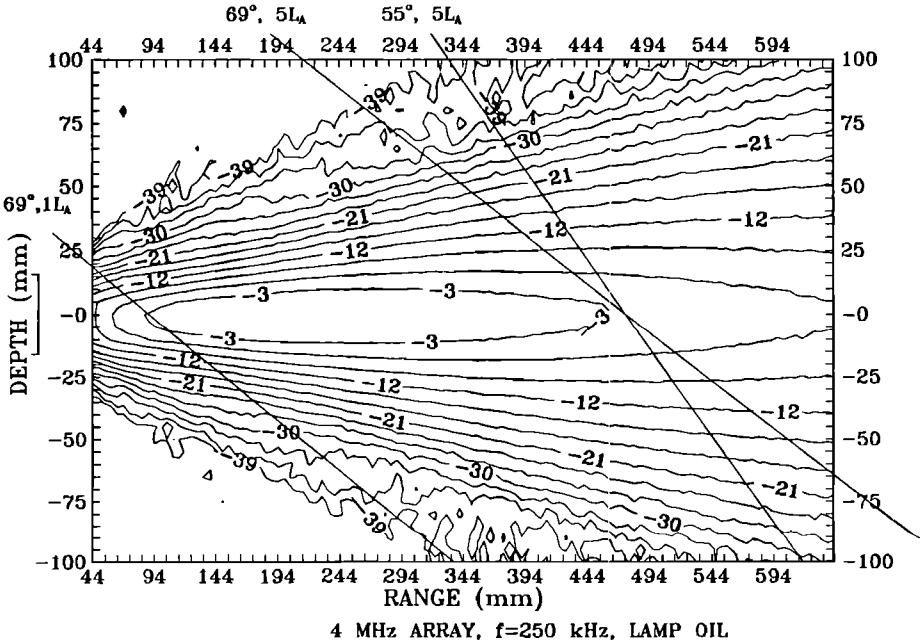


FIG. 2. Map of pressure level contours of the incident field in lamp oil. The levels differ by 3 dB, and are referred to the maximum level within the frame. Contours below $-39$ dB are suppressed. The primary frequencies are 4.15 and 4.4 MHz, giving secondary frequency sound of 250 kHz. The primary source is indicated to the left of the frame. The three straight lines indicate the position of the interface for some cases shown in Fig. 4.

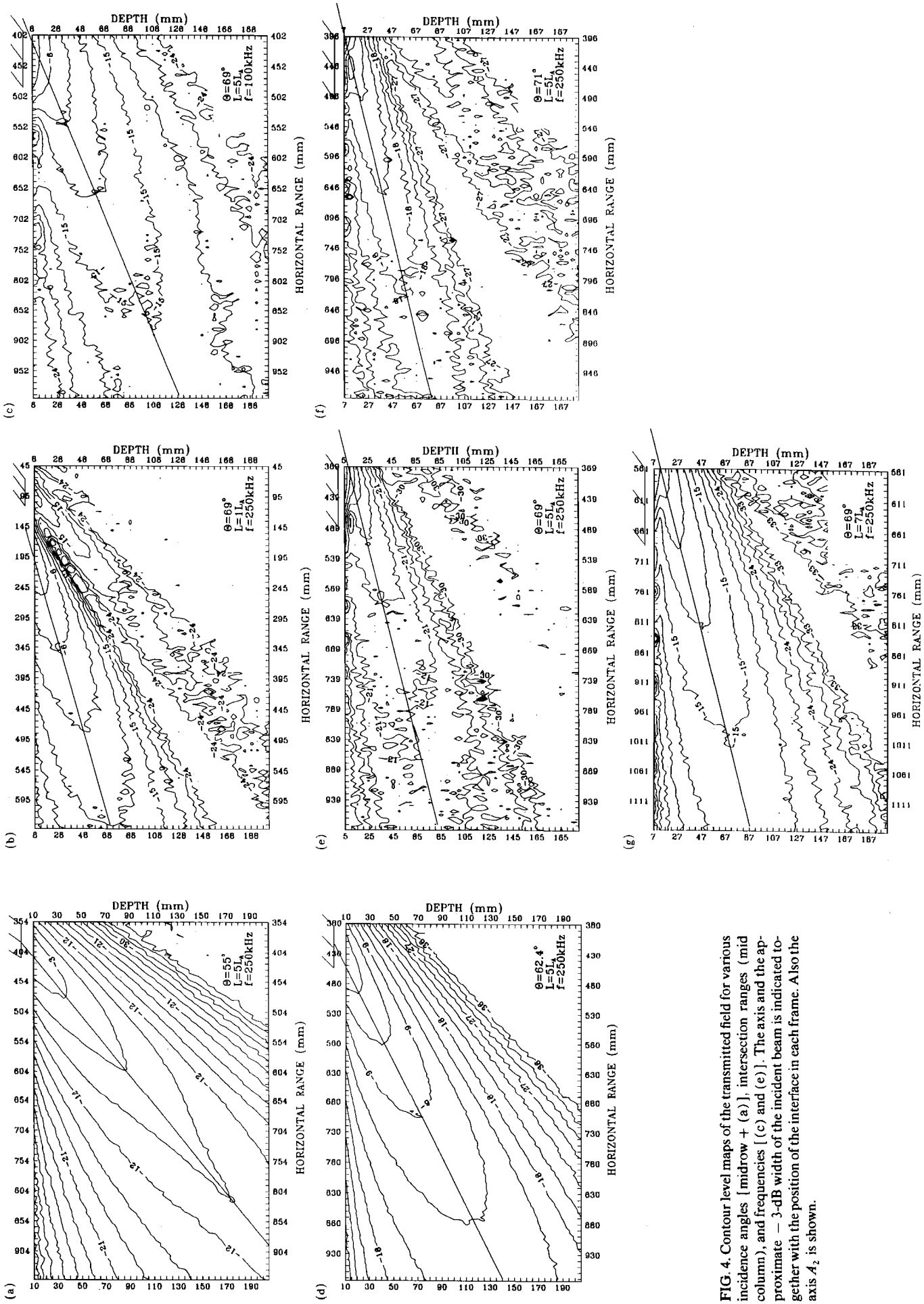


FIG. 4. Contour level maps of the transmitted field for various incidence angles [midrow + (a)], intersection ranges (mid column), and frequencies [(c) and (e)]. The axis and the approximate − 3-dB width of the incident beam is indicated together with the position of the interface in each frame. Also the axis $A_2$ is shown.

different values of incidence angle $\theta$, intersection ranges $L$, and difference frequency $f_-$. Figure 4 presents contour maps of the field obtained for representative values of these parameters, keeping all but one parameter constant. In each frame the contours are plotted for 3-dB steps in the pressure amplitude level, which is normalized to 0 dB at the maximum level in each frame. In order to not obscure the essential features, the contours below a certain level are suppressed. In each frame, the location of the interface and the incident beam is shown—the latter by its axis ($A_1$) and $-3$-dB radius. The mapped field starts at slightly different depths below the interface. Also indicated in each frame is the asymptotic axis of the main penetrating lobe, i.e., $A_2$ in Fig. 1.

The central horizontal row—with the addition of the upper left frame (a)—shows varying incidence angles, and the central vertical column varying intersection ranges. The upper right frame (c) together with the central frame (e) shows the effect of changing frequency. The directivity of the parametric array is relatively insensitive to changes in the difference frequency,[16] which indicates that the difference between frame (c) and (e) is mainly due to the change in wavelength.

The penetrating main lobe can easily be seen in each frame, even at the highest incident angles. Some frames show the presence of what will be referred to as "underlobes," especially at high incidence angles. These are lobelike structures where the pressure amplitude is rising above the noise level and indicates sound penetration at steeper angles than the mainlobe. Another interesting phenomenon is the series of small minima and maxima seen along the interface in some of the frames, especially at high incidence angles. A similar series of fluctuations can be seen between the mainlobe and the first underlobe in frame (b), and to some extent also between first and second underlobe. One should also observe the sharp fall of the amplitude of the mainlobe just beneath the interface, for example in frame (e), and the much slower decay of amplitude with depth below this.

Figure 5 shows the measured angle of refraction $\theta_A$ of the main beam as a function of incidence angle $\theta$, for $L = 475\ \text{mm} = 5L_A$ and $f_- = 250$ kHz. For comparison, computed results from Ref. 5 are also plotted. These are obtained for slightly different parameters: A Gaussian amplitude distribution (along the interface), with $ka = 5.9 - 26.6$, and critical incidence angle 60.7°. These curves should therefore have been shifted 1.7° to the right to correspond with the experimental data at the critical angle. The plane wave refraction (Snell's law) is also shown. In the experiment $ka \sim 17.5$. The dependence of refraction angle with intersection range is shown in Fig. 6 for $\theta = 69°$ and $f_- = 250$ kHz. The dependence is not very strong, but clearly $\theta_A$ increases with range. Frequency is found to have a much stronger influence, as presented in Fig. 7, for $\theta = 69°$ and $L = 5L_A$. Within the range investigated (100—250 kHz), the refraction angle increases almost linearly with frequency.

In Fig. 8, we present the sound level of the refracted mainlobe versus depth for several cases. The basic parameters are $\theta = 69°$, $L = 5L_A$ and $f_- = 250$ kHz, and the value of a changed parameter is indicated next to the corresponding curve, which is fitted to the data. The sound level was measured along the least steep descent of the mainlobe and individually normalized to the maximum level in each case. For reference some of these levels are compiled in Table II. Observe that the shallowest depth differs somewhat from case to case. As expected penetration decreases with increasing incidence angle. Note also that penetration tends to increase with increasing intersection range and decreasing frequency.

The observed displacement $\Delta A$ of axis $A_2$ with respect to

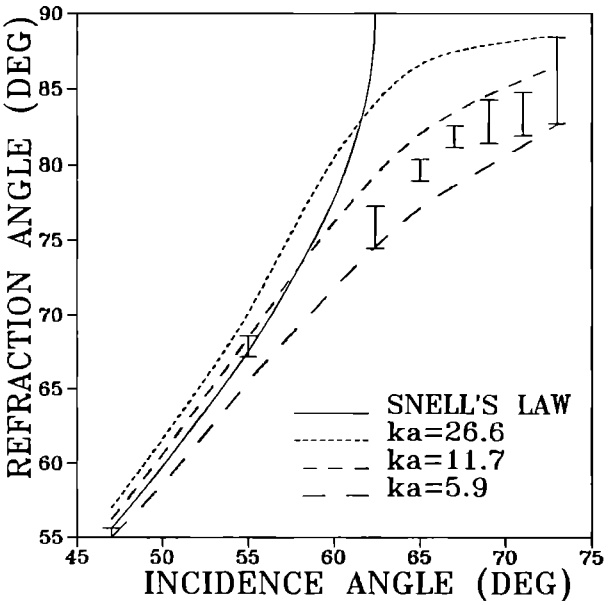


FIG. 5. Refraction angle $\theta_1$ as a function of incidence angle $\theta$ for $L \approx 5L_1$ and $f_- = 250$ kHz. The curves show theoretical results for plane waves (Snell's law) and for a Gaussian source distribution along the interface according to Naze Tjótta *et al.*[5] In the experiment, $ka \sim 17.5$.

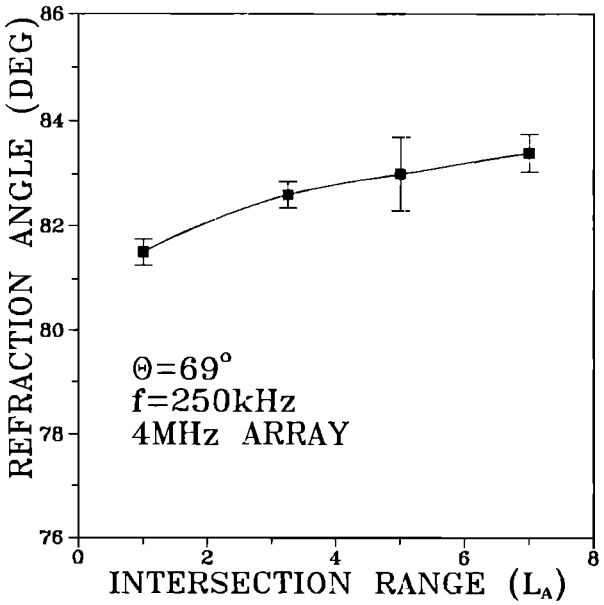


FIG. 6. Refraction angle as a function of intersection range $L$. The curve is fitted to the data.

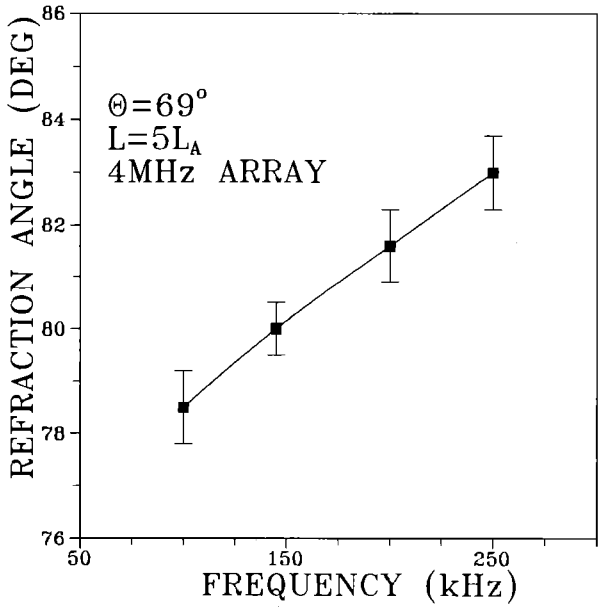


FIG. 7. Refraction angle as a function of frequency. The curve is fitted to the data.

$A_1$ on the interface is shown in Figs. 9 and 10. In Fig. 9, the incidence angle is varied at $L = 5L_A$ and $f_- = 250$ kHz, and we note that the displacements are all negative, i.e., toward the primary source. This is not always the case, however, as seen in Fig. 10. Here, the incident angle is fixed at 69°, while the range $L$ is varied. The frequency is 250 kHz, except for three data points at $L = 5L_A$ where $f = 100$, 145, and 200 kHz, respectively. For $L \leqslant 3L_A$, the displacement is seen to be positive. Also, at least at a range $L \sim 5L_A$, we

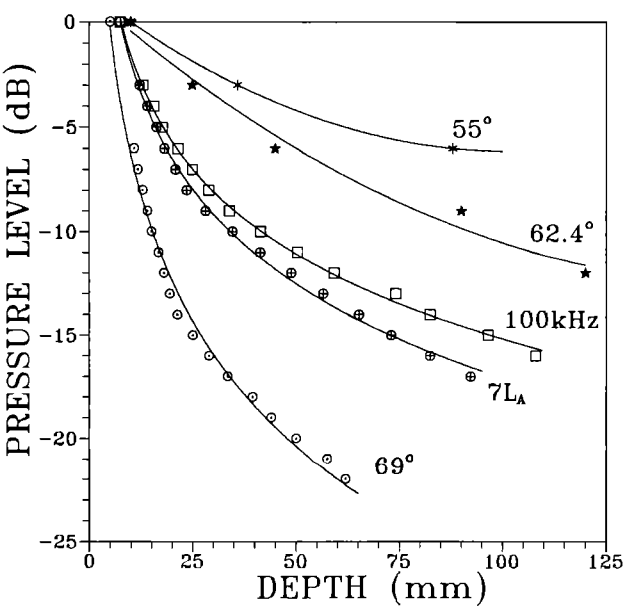


FIG. 8. Sound level as a function of depth in the least steep descent path of the main penetrating beam for the 4-MHz array. The curves are best fits to the data points. The reference level is put to 0 dB at the shallowest depth. Except for the parameter given next to each curve the parameters are: $L = 5L_A$, $f_- = 250$ kHz, $\theta = 69°$.

TABLE II. Highest amplitude levels as a function of incidence angle for $L = 5L_A$ and $f_- = 250$ kHz for the 4-MHz array. Note that the shallowest depth was not the same in all cases.

| $\theta$ | 47° | 55° | 62.4° | 65° | 69° | 71° |
|---|---|---|---|---|---|---|
| Level (dB) | 0 | − 1.3 | − 2.9 | − 8.9 | − 14.1 | − 22.7 |

observe that the displacement is not very sensitive to the frequency.

### B. 2-MHz array

A map of the incident field is shown in Fig. 11 as a section in the horizontal plane, with the axis oriented horizontally. If we assume axial symmetry, this map is also representative for the vertical section. A typical profile along the interface is shown in Fig. 12. Curiously enough, there seems to be a tiny sidelobe around 35–37 dB below the maximum also in this case, even if this type of parametric array is not expected to show such (it belongs to the parameter region II—see Appendix).

In these measurement series the accuracy in the primary source height was $\Delta H = 0.5$ mm and in the incidence angle $\Delta\theta = 0.25°$. The accuracy of the hydrophone position was $\Delta x = 1.5$ mm, $\Delta y = 1.5$ mm, and $\Delta z = 2.5$ mm. The systematic error in $y$ position is increasing from 0 mm to maximally $\pm$ 1 mm at the end of every second depth trace, as for the 4-MHz array.

The measurements were conducted as for the 4-MHz array, except that this time the height $H$ of the primary source above the interface was kept constant for most of the runs, while the incidence angle was varied. Thus for example with $H = 80$ mm the range from the primary source to the interface increased from $L = 0.42L_A$ at $\theta = 65°$ to $L = 0.69L_A$ at $\theta = 75°$. The spot size remains roughly the same at these ranges, and $ka \approx 7.1$ where $a$ equals the − 3-

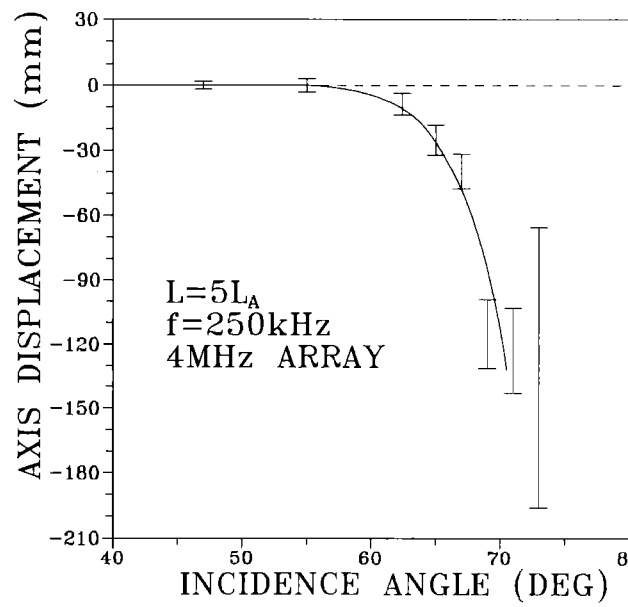


FIG. 9. Axis displacement as a function of incidence angle. The curve is fitted to the data.

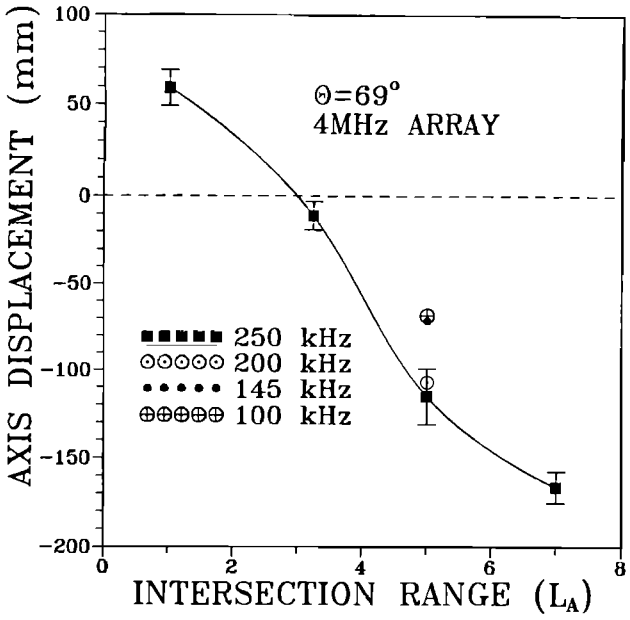


FIG. 10. Axis displacement as a function of intersection range $L$. The curve is fitted to the data.

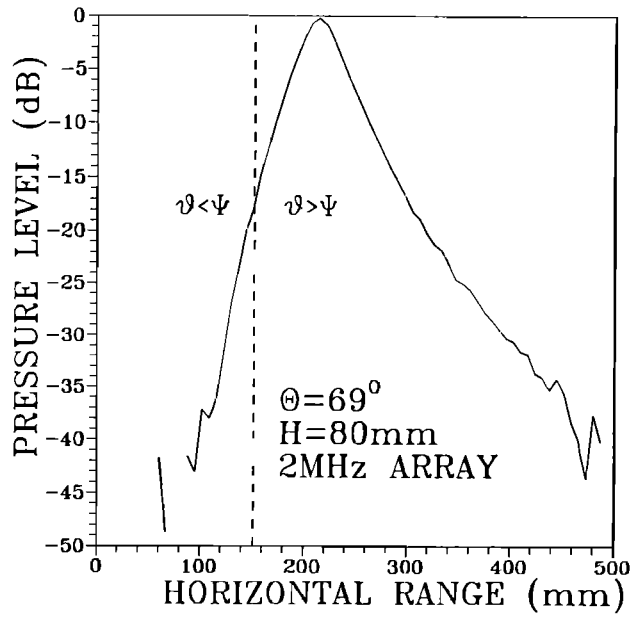


FIG. 12. Profile of incident field along the interface for the 2-MHz array. Ranges to the right of the vertical dotted line correspond to incidence angles greater than the critical angle, denoted Ψ in this figure.

dB radius of the beam, and $k$ is referred to the lower fluid (water).

Figure 13 presents the mapped field for four cases of interest. In frame (a), $H = 154$ mm that corresponds to $L = 0.95L_A$ at $\theta = 69°$. Thus the situation here is comparable to the case shown in Fig. 4(b) (except, of course, for the difference between the two arrays). Inspection shows that the axis of the main beam in Fig. 13(a) has negative displacement, in contrast to Fig. 4(b). Further, both cases show one marked underlobe, which seems to be an extension of the incident beam in the 4-MHz case, but is coming from a region lying closer to the source in the 2-MHz case. Note also that the amplitude is higher in the underlobe than in the mainlobe just beneath the interface in Fig. 13(a), and that penetration of for example the − 15-dB contour is deepest in the underlobe. This contrasts the situation in Fig. 4(b), where the highest amplitude and deepest penetration is found in the mainlobe. In both cases, interference minima are seen between mainlobe and underlobe.

Figure 13(b) shows the same situation with $H = 80$ mm, i.e., at about only half the range of above. Here, there is a marked difference from frame (a) to be seen, and the situation corresponds quite well to the one seen in Fig. 4(b) (recall, however, that in this case the primary waves are still quite strong as they reach the interface, and that they are almost at the outermost axial maximum).

Frame (c) and (d) show the field at 71° and 75° incidence, respectively. At 71° the highest amplitude and deepest penetration is again found in the underlobe. At 75° penetra-

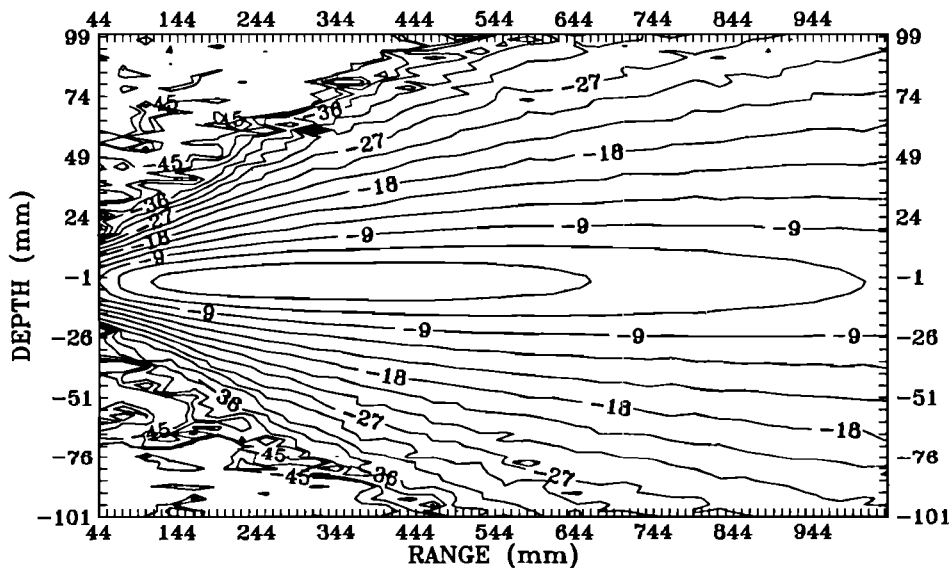


FIG. 11. Incident field of 2-MHz array at 250-kHz difference frequency (horizontal section). Contours differ by 3 dB. Contours below − 45 dB referred to the maximum level are suppressed.

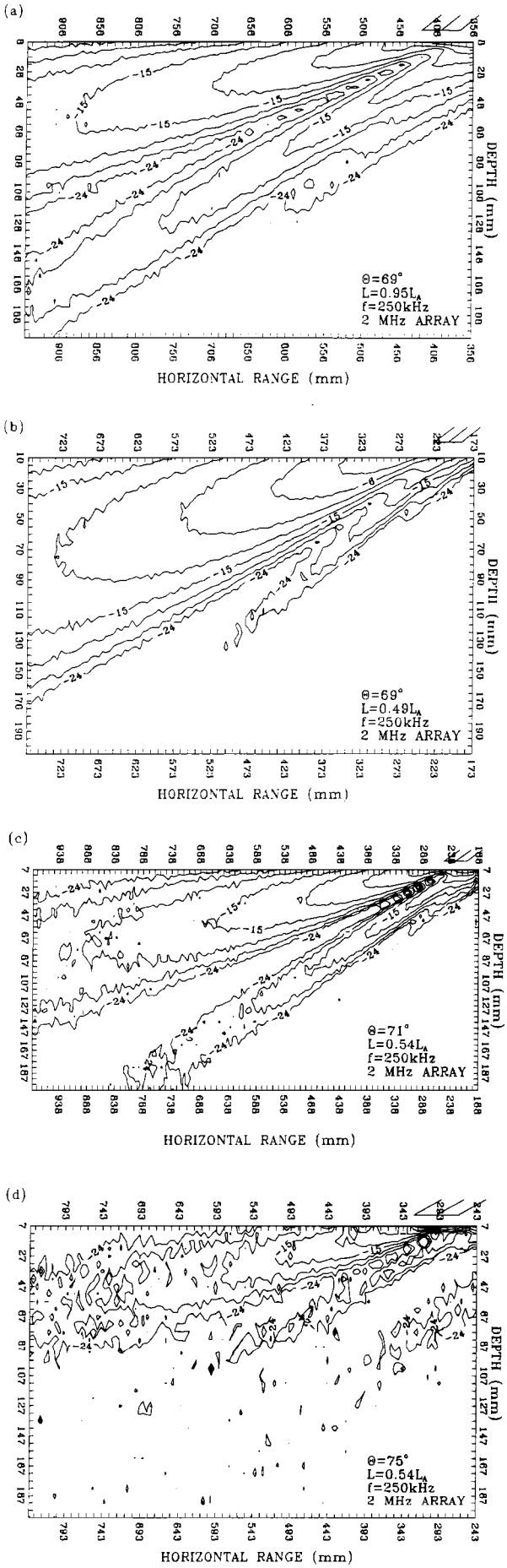


FIG. 13. Contour level maps of the transmitted field for the 2-MHz array.

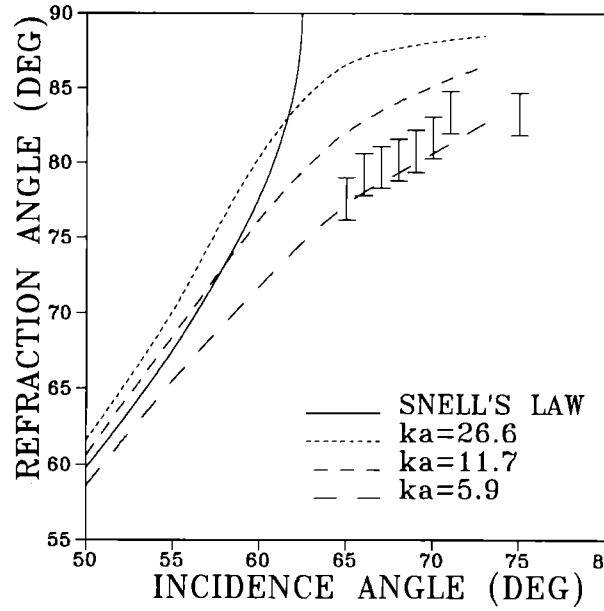


FIG. 14. Refraction angle $\theta_A$ as a function of incidence angle $\theta$ for the 2-MHz array, with constant source height $H = 80$ mm at $f = 250$ kHz. The curves show theoretical results for plane waves (Snell's law) and for a Gaussian source distribution along the interface according to Naze Tjøtta *et al.*[5] In the experiment, $ka \sim 7.1$.

tion is generally very weak, but the mainlobe dominates. Along the interface periodic fluctuations may be distinguished.

Figure 14 shows the measured refraction angle $\theta_A$ for $H = 80$ mm, $f = 250$ kHz and $0.45L_A < L < 0.7L_A$. Also here the curves represent Snell's law, and results from Ref. 5 subject to the same reservations as given for Fig. 5. It is interesting to note that the measurements of $\theta_A$ correspond even more closely to the linear theory in this case.

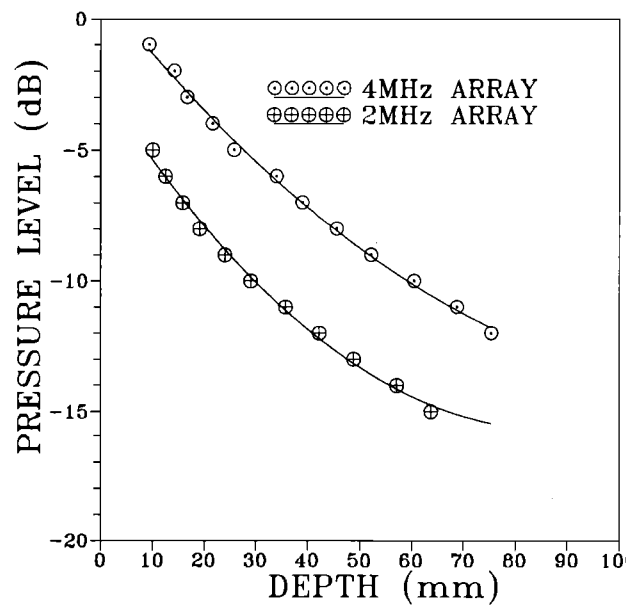


FIG. 15. Sound level as a function of depth in the least steep path of the main penetrating beam at $L \sim 1L_A$ for 2- and 4-MHz array at 69° incidence. Levels are referred to the shallowest depth in each case. The curves are fitted to the data.

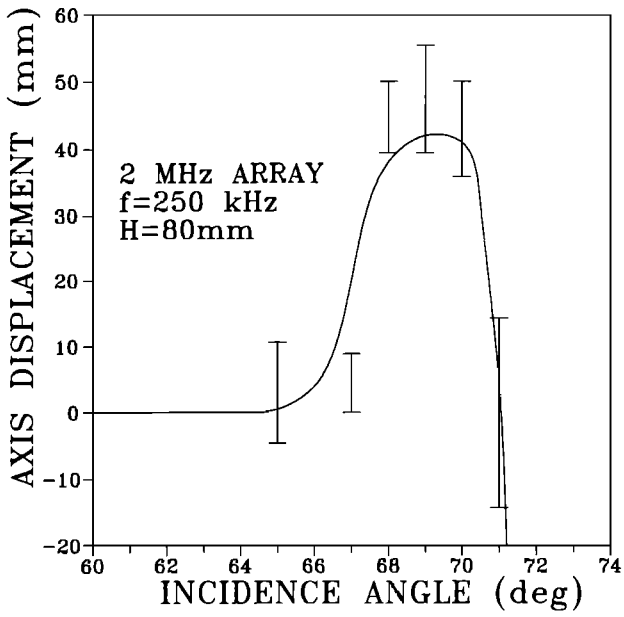


FIG. 16. Axis displacement as a function of incidence angle for the 2-MHz array. The curve is fitted to the data.

Figure 15 shows the sound level of the transmitted main beam in a similar fashion to Fig. 8. The frequency is 250 kHz, and for comparison results from the 4-MHz array at the same intersection range and incidence angle is included in the figure. Penetration is significantly deeper with the 4-MHz array.

Figure 16 shows the displacement $\Delta A$ of the main axis of the transmitted beam, as a function of incidence angle for $f_- = 250$ kHz. Observe the curious peaking of $\Delta A$ near 69°, and that for higher incidence angles the displacement becomes negative. This behavior is markedly different from the observations with the 4-MHz array.

## III. DISCUSSION

In this section, we discuss the observed features of the transmitted field starting just below the interface and successively progress downward. Finally, we discuss the nature of the responsible mechanism(s).

### A. Evanescent wave field

We start by drawing attention to the series of fluctuations seen just beneath the interface in many cases, only some of which are included here. At first, we were inclined to believe that these were due to reflections between hydrophone and interface, which also Wingham *et al.*[7] mentions. However, this explanation is hardly likely. Consider, for example, in Fig. 4(e) the strong minimum just beneath the far edge of the incident beam that lies deeper than those seen further out. Observe that in this region, the transmitted field decays quite rapidly with depth, while this decay takes place at a slower rate as one goes deeper. We attribute this rapidly decaying field with depth to evanescent waves connected with the reflected field. The evanescent waves propagate with wave fronts perpendicular to the interface at a speed that is less than the sound speed in the lower fluid, and are continuously reradiated into the reflected field. Therefore, their amplitude decays with increasing range, as well as with depth, where the decay is exponential. Thus the fluctuations are most likely due to interference between the evanescent waves and the transmitted beam. The minima can occur only where these two waves are of nearly equal amplitude, and therefore lie deeper where the penetrating field is strong, which it is in particular just beneath the spot. In favor of this interpretation is also the fact that such interference is seen in some relevant theoretical results.[7,17] In Ref. 17, the transmitted field from a point source reveals a series of fluctuations similar in nature to those observed by us.

In some cases, this interference is so strong that the usual definition of the acoustic axis of the main beam becomes meaningless in that region, as for example in Figure 4(f). In other cases they seem not to be present, however, although this is most likely due to the shallowest trace having been taken too deep. It seems that the interference minima are shifted toward the interface if the transmitted main beam is strong and the evanescent wave field is weak, as for example at $\theta \leqslant 62.4°$, or evidently when $L < L_A$.

Figure 8 indicates typical ranges for the penetration depth of the evanescent waves, which can be characterized by the decay length $\mathscr{L}$, defined by $e^{-z/\mathscr{L}}$. It is clear that $\mathscr{L}$ must be in the range 10–20 mm for $5L_A \leqslant L \leqslant 7L_A$ at 69° incidence. However, a simple calculation based on Snell's law shows that to obtain $\mathscr{L}$ in this range the incidence angle must be less than 63°. Near critical incidence (62.4°) $\mathscr{L}$ is extremely angular dependent, of course, while for angles above 63° it varies less strongly. At 69°, we find $\mathscr{L} = 2.9$ mm, which obviously could not have been observed with this experiment. Thus the mean contribution to the evanescent wave field comes from waves in the incident beam very close to, but above the critical angle.

### B. Mainlobe

Beneath the evanescent wave field, the mainlobe appears clearly in all cases observed. Although strong underlobes are sometimes seen there is never a doubt as to where the main transmitted energy is to be found.

Starting at incidence angles below critical, we notice a peculiar peaking of the contour levels along the axis, as in Fig. 4(a). This is seen in several cases and is quite consistent. We have, however, no explanation for this. At short intersection ranges $L < L_A$ pseudosound could be a candidate, generating difference frequency signals directly in the hydrophone as it is being exposed to the primary field (recall that at subcritical incidence the primary field too is transmitted into the lower fluid). However, we do not see any signs of pseudosound when the incident field is mapped at even closer ranges, like in Figs. 2 and 11, and besides, the primary field is negligible when $L = 5L_A$. Since the transmission coefficient varies strongly with incidence angle in this region the transmitted beam is highly asymmetric, which is easily seen from the figure, but it is highly unlikely that this effect alone is responsible for the peaking of the contour levels. Whatever the explanation might be, the effect disappears at and above critical incidence angle.

The refraction angle $\theta_A$ of the main beam as a function of incidence angle fits within reasonable limits predictions from the theory of Naze Tjøtta and Tjøtta,[5] although the parameters they used were not obtained exactly in the experiment. Surprising as this may be, the fit is even better for the 2-MHz array results. Wingham *et al.*[7] presents no predictions of this relationship. The more recent theoretical works[10,11] defines the acoustical axis in a way which is difficult to apply to experimental results, namely as the curve connecting amplitude maxima along horizontal traces. Due to noise fluctuations always present in experimental data this method provides inconsistent results. Our approach, applying least steep descent, is much safer on noisy data since this effectively corresponds to correlation in two dimensions instead of one. For large incident beam angles these two definitions differ significantly: For example, in Fig. 4(d) at critical incidence the axis determined according to their definition is about 3° steeper than what we find. This discrepancy propagates to axis displacement also, of course.

In Ref. 5, a different axis definition was employed where maxima located on concentric circles centered at the spot center was joined. This approach differs only marginally from ours except close to the interface, and yields the same asymptotic acoustic axis.

The refraction angle $\theta_A$ does not depend strongly on intersection range, as shown in Fig. 6, although there is a clear tendency to steeper refraction at shorter ranges. This is also reflected by comparing Figs. 5 and 14.

The decrease of $\theta_A$ with frequency evident in Fig. 7 is no surprise. Lowering the frequency effectively reduces the directivity of the array, and thus more energy becomes available at subcritical conditions leading to steeper penetration.

The depth dependence of the main beam amplitude along the axis show that all curves in Fig. 8 seem to be more or less curved all the way, while according to Ref. 11 the decay of the main beam amplitude with depth is expected to be nearly linear. Thus we should expect to see a transition from the exponential decay of the evanescent waves to a more slow linear decay further down. Several of the curves show a tendency to such behavior, for example those at $7L_A$ and 100 kHz, but evidently the measurement range is too small that this can be confirmed with certainty. The fact that the amplitudes are not taken vertically but along an inclined curve that is not necessarily straight, especially close to the interface, also tends to obscure the transition from evanescent to transmitted wave field. It is interesting to notice that even at subcritical incidence (55°), the curve is not a straight line, signifying the presence of evanescent waves caused by the postcritical part of the incident beam. Moreover, the curves at the three different incidence angles demonstrate how the amplitude of the main beam decays at a more rapid rate with depth at higher incidence angles. To get a measure of how the absolute levels vary the normalization levels for each curve must be adjusted according to Table II.

It is interesting to note that increasing the intersection range, or decreasing the frequency, seems to increase the penetration depth. The latter corresponds with the steeper refraction angle observed at lower frequencies. However, as already commented, the refraction angle increases slightly with increasing intersection range. Still, the amplitude penetrates deeper in this case. We are reluctant to conclude from this, however, that increasing the intersection range in general leads to increased penetration depth, for the following reason. The contribution from the evanescent waves is very important in the normalization of these curves, both concerning their amplitude at the shallowest depth and their decay constant $\mathscr{L}$, which we already have shown is very angular dependent. Accordingly this contribution must be very sensitive to the angular distribution of the incident beam. However, the accuracy in the primary source attitude ($\pm 0.1°$) does not permit repeatability of the tilt angle to the precision that may be required to eliminate variations in the evanescent wave field. Thus we can not rule out that this factor is the dominant one.

Next we discuss displacement of the asymptotic transmitted axis $A_2$ with respect to the incident. As Figs. 9–10 show the displacement is negative for all cases where $L > 3L_A$. Physically this is easy to explain from the following simplistic model. The wave field that contributes to the main transmitted beam must be incident below critical incidence. The rays corresponding to these angles hit the interface on the source side of the beam center. Thus the axis $A_2$ should intersect the interface in this region, i.e., negative displacement, which increases with incidence angle, as in fact is observed. In terms of lower fluid wavelengths the displacement at 70° incidence corresponds to 20 wavelengths. References 10 and 11 report that a positive axis displacement of maximally one-half wavelength is to be expected if certain conditions are met, but such a small displacement would not have been resolved in our experiment. At $L = 1L_A, \theta = 69°$ we do, however, observe a positive displacement of 10 wavelengths, and with the 2-MHz array at intersection ranges $\sim 0.5L_A$ the displacement is positive at all incidence angles, Fig. 15. Based on linear theory this displacement is hard to explain. However, in these cases the primary beams are still quite strong at the interface, and as mentioned in the Introduction, the truncation of the array by the interface leads to progressively smaller virtual source apertures with range in the intersection region. Radiation from these source apertures is less directive than the free-field ones, and contribute therefore to the wave field below critical incidence. At the same time, they are located mainly on the far side of the beam center, and thus may shift $A_2$ in positive direction. Second, the primary waves are reflected in this area (recall that they also may undergo a positive axis displacement upon reflection[18]). At the interface, the nonlinear boundary conditions lead to a source distribution that also contributes to the transmitted field. It remains to be investigated which of these effects (if any) is the dominant one. Anyway, it is likely that the positive displacement signifies the presence of nonlinear effects.

### C. Underlobes

Except at $L = 1L_A$ the 4-MHz array shows evidence of a weak underlobe 25–30 dB below the maximum level in the frame. This underlobe seems to originate in a region outside the frames closer to the source, and we believe it is connected

to the rudimentary sidelobe seen in the incident field. Its level, axis direction and its place of intersection with the interface all support this. For the incidence angles presented here the sidelobe is subcritical. Therefore at increasing incidence angles its relative importance also increases, as seen for example in Fig. 4(f) at 71°.

However, the underlobe structure at $L \leqslant 1L_A$ is radically different from this for both arrays. Sometimes weaker underlobes below the first are seen [Fig. 13(c)]. The first underlobe can be quite strong, and occasionally have a higher amplitude and deeper penetration than the main lobe [Fig. 13(a) and (c)], although it is clearly much narrower. It seems to originate in a region on the interface close to, but on the source side of the beam center. The interference minima between main beam and underlobe can be seen in all the frames, as is to be expected whenever two wave fields of the same frequency propagate in different directions in the same region of space. The actual locations of the minima are dependent both on the amplitude and phase distribution in the two fields, and have not been investigated.

It seems obvious at this point to conclude that the underlobes somehow are caused by nonlinear effects due to the primary beams being intersected by the interface. Wingham *et al.*'s theoretical results[7] show qualitatively the feature of underlobes, without interference fluctuations. In addition to their model, we propose several other candidates, which will be discussed in the next section.

### D. Linear and nonlinear mechanisms

First, we address the problem whether transmission at postcritical incidence angles is a linear or nonlinear process. In Sec. I, we stated that if postcritical transmission is observed with parametric arrays at $L > 3L_A$, which is indeed demonstrated to be the case, then the process must be of linear nature. As discussed above, however, the structure of the field is markedly different if $L \leqslant 1L_A$ where still strong primary waves are intersected by the interface. This structure change is difficult to explain by purely linear processes, and opens the possibility for contributions from nonlinear effects. Thus we are led to conclude that postcritical transmission is mainly a linear process, but that when parametric arrays are used nonlinear effects may contribute to the transmitted field if the primary waves are intersected by the interface. With the aim to clarify the physical processes involved in postcritical transmission, we are proceeding with a discussion of both the linear and the nonlinear case.

The details of the linear mechanism can be outlined as follows. A beam of sound can be resolved into plane waves propagating in slightly different directions, the amplitude and phase distribution of which represents the angular spectrum. The angular spectrum is obtained by taking the two-dimensional spatial Fourier transform of the source distribution, which is well known to correspond with the far-field directivity pattern. The modulus of the angular spectrum is range invariant (except closer to the source than a few wavelengths, where evanescent waves may occur), but the phase is not, of course. In the far field, the directivity pattern is also range independent; at a fieldpoint here only waves propagating along the direction from the source center are found—in other words, the source may be regarded as a point. However, in the near field the beam structure does vary with range. This is because in this region waves of different directions overlap, i.e., through a fieldpoint waves of different directions pass. The source can no longer be regarded as a point, and since the solid angle spanned by the source is range dependent, the actual beam structure (which results from superposition of all waves) is range dependent too. Although the above argument is based on plane sources it is easily extended to volume sources like the parametric array. The modulus of the angular spectrum is still range independent outside the source region (if we neglect evanescent waves and situations where the source is nontransparent so that range-dependent shadow effects may occur at certain directions).

Thus the field of a sound beam can be regarded as a bundle of waves of slightly different directions centered around the beam axis. Upon intersecting an interface with the beam axis at postcritical angle some waves may still be at subcritical incidence, and will be transmitted according to classical theory, while the postcritical part of the beam is reflected (yet causing evanescent waves below the interface). The transmitted (and reflected) field may be obtained by applying the transmission (reflection) function as a filter for the incident wave field, i.e., as a product of the angular dependent coefficient and the angular spectrum of the incident field. However, in reconstructing the field in real space the phase must be taken into account, and accordingly the transmitted (and reflected) waves depend both on the range between source and interface, and the angular spectrum. This consideration applies, of course, even if intersection takes place in the far field of the beam. Another way to see this is to consider how the insonified spot size varies with range, although the angular spectrum is constant.

In their first approach to treat the transmission problem Naze Tjøtta and Tjøtta[5] concentrated on the amplitude and phase distribution of the spot, which was taken as a new source to replace the incident beam. Their results indicate that postcritical transmission occur largely if the $ka$ value of the spot is moderate, while their approximation is valid only if $ka \gg 1$. This approach is perfectly valid, but unfortunately it has focused higher attention to the $ka$ value of the spot rather than the source. This again has led to some confusion as to what is a "narrow beam." In particular, Jensen and Schmidt[8] by calculating the angular spectrum of a focused sound beam show that the beam with the smallest spot size has the broadest spectrum. This is correct, of course, for a focused beam. However, they also refer to this as the most narrow beam—referring to the spot size—and thereby conclude that "it is a contradiction to state that narrow beams are highly directional." This is correct only for focused beams where the focal diameter is used to express its narrowness. For ordinary beams it is quite appropriate to use the term "narrow" on highly directive beams, as usual. On the other hand, to obtain a directive beam the source dimension has to be large compared to the wavelength, and thus nowhere will the beam present a small-sized spot at the interface, if the source is plane. The parametric array is somewhat special in that it can provide a beam that is both narrow in

directional sense and can produce a small spot.

According to this discussion, the spot size is not essential for obtaining postcritical transmission. It is clear, however, that as the spot size increases due to geometrical spreading the actual width of the main transmitted beam also grows, leading to reduced amplitude although its angular spectrum remains essentially unchanged. Thus, in order to obtain a transmitted field that is spatially confined, and thus relatively strong, it is necessary to make the spot as small as possible.

Experiments on postcritical transmission with ordinary sound sources are to our knowledge only reported by Muir *et al.*,[1,2] with negative results, and by Berktay and Moustafa[4] with positive results. So far we have only made temporary measurements, but these indicate that postcritical transmission is possible also with ordinary sound sources.

We now turn to the nonlinear case. Here, several mechanisms must be considered. The scenario consists of the primary waves of the parametric array intersecting the interface at postcritical incidence. Thus we have to consider (1) the effects of array truncation as suggested by Wingham;[6] (2) nonlinear interactions between incident and reflected beams where they overlap; (3) nonlinear terms in the boundary conditions, which may act as a new source located on the interface; (4) interactions between evanescent waves connected with the reflected primary beam; and (5) transmitted primary waves.

(1) Wingham[6] presents a physical interpretation of his model that is difficult to follow. We interprete the essentials of this model as follows. For simplicity we stick to his assumption of a primary field in the form of a collimated plane wave. The difference frequency field can be regarded as radiated by a continuous distribution along the beam axis of virtual sources with aperture equal to the primary beam cross section, and phased corresponding to a plane wave of difference frequency propagating along the axis. (We have previously obtained excellent agreement for the axial field by using this model.[14]) Thus each virtual source has radiating characteristics like the primary source at the difference frequency. However, if the beam is intersected obliquely by a (nonpenetrable) plane, the source apertures get progressively smaller, and thus radiate with less directivity (and source strength). Their contributions tend to widen the angular spectrum of the difference frequency beam, and thus may increase the transmission. Note that this source region is of very limited extent, but this is compensated to some extent by its closeness to the interface that reduces geometric attenuation. We have not undertaken to code Wingham's theory, and Wingham *et al.*[7] provide few results general enough to be compared to other experiments than their own. However, as already pointed out they obtain good correspondence between theory and experiment, and their results show both the interference with the evanescent wave field and several underlobes. Thus this mechanism is a likely candidate for explaining nonlinear transmission, but a detailed comparison between theory and experiment is necessary to judge its relevancy with respect to other possible mechanisms.

(2) Nonlinear interaction between noncollinear beams is still a controversial theme, but it has been shown lately[19] that such interaction may occur. If we follow a virtual elementary source in this configuration it moves along a path parallel to the interface at supersonic speed, reradiating at Doppler angles equal to the incident and reflected beam. However, to calculate the resulting field is extremely difficult—recall for instance that there are actually two sets of interacting beams—and with regard to the marginal signals so far obtained with crossed beams we are inclined to assume that this effect is negligible.

(3) Usually boundary conditions at the source are linearized with good results even in nonlinear circumstances because the field resulting from the higher-order terms is not cumulative, in contrast to interactions taking place within the propagating wave field. Here we are concerned, however, with the field rather close to the source in question, which is the spot itself. Thus one cannot disregard contributions from nonlinear boundary conditions off hand, but we are not in the position to evaluate this field here.

(4) Contributions from the evanescent wave field of the reflected primary waves can be disregarded right away, but are mentioned here for completeness. These waves propagate at subsonic phase velocity and, if they interact, can only reradiate into the upper fluid.

(5) Although the angular spectrums of the primary beams are extremely narrow there is inevitably some energy at subcritical incidence, however small. This wave field will be transmitted to the lower fluid, where nonlinear interactions continue, and must be considered as a possible contributor to the transmitted difference frequency field. However, in this experiment the $ka$ values are of order $\sim 300$ and $\sim 100$ for the 4- and 2-MHz array, respectively. Thus, at 69° for example, the transmitted part of the spectrum lies outside the 10th and 4th sidelobe, giving amplitudes $\sim 30$ dB and $\sim 20$ dB below the incident field, respectively. This implies a reduction of source strength of more than 40 dB, which indicates that significant contributions from this field are highly unlikely.

Thus we conclude that the most likely nonlinear mechanisms that may contribute to the transmitted field are primary beam truncation, and nonlinear boundary conditions at the interface, the former being the strongest candidate at present.

## IV. SUMMARY AND CONCLUSIONS

The purpose of this article is to present results from an experiment on the transmission of a sound beam at and above critical incidence on an interface between two fluids. The two fluids (oil and water) were chosen to simulate closely a water/sand interface. The incident beam was produced from a parametric array that was arranged to intersect the interface either within the absorption limit of the primary waves, or far outside the same, with the aim to discriminate between linear and nonlinear processes active in the transmission.

The results show that postcritical transmission is basically a linear process, and was observed up to about 10° above critical incidence. Moreover, interference between the

transmitted field and evanescent waves was observed close to the interface. The asymptotic axis of the main penetrating beam was investigated with respect to refraction angle and beam displacement. In a linear situation only displacement directed toward the projection of the primary source on the interface was observed. A small sidelobe seen below the mainlobe is attributed to a rudimentary sidelobe in the incident beam.

The field structure becomes markedly different, however, if the primary waves are intersected by the interface. The main difference is the presence of a strong "underlobe" that has no direct counterpart in the incident field as measured in free field. Interference is observed between this and the mainlobe. In addition, an axis displacement away from the projection of the primary source is sometimes seen. This change in field structure is attributed to nonlinear effects, the candidates of which are discussed in detail. The most likely of these are the effects of primary beam truncation suggested by Wingham,[6] and nonlinear boundary conditions at the interface where the primary beams are intersected.


## ACKNOWLEDGMENTS

The authors wish to thank Professors J. Naze Tjøtta and S. Tjøtta for many stimulating discussions throughout the work on this experiment. They also wish to acknowledge the assistance of Erich Carr Everbach of Yale University in providing data on the sound speed and nonlinearity parameter of the "lamp oil" used in this experiment. Support for the experiment was provided by the Norwegian Research Counsel for Science and Humanities.


## APPENDIX

It is illustrative to categorize parametric acoustic arrays with respect to the parameters introduced by Vestrheim,[20] which are repeated below for convenience. In terms of the source radius $a$, array length $L_A$ and the wavenumbers $k_a$ and $k_-$ of the highest primary frequency and difference frequency, respectively, these are

$$N_f = k_-/k_a,$$

$$N_F = \sqrt{k_a L_A}/k_a a,$$

$$N_A = k_a a/\sqrt{k_- L_A} = \sqrt{N_f}/N_F,$$

$$N_D = \sqrt{k_- L_A}/k_a a = \sqrt{N_f}\cdot N_F.$$

Here, $N_F$ effectively measures whether nonlinear interaction takes place only in the near field of the primary waves ($N_F < 1$) or also extends into the far field ($N_F > 1$). Any parametric array is uniquely located in the plane spanned by $N_f - N_F$. In this plane $N_A = 1$ and $N_D = 1$ correspond to curves that effectively divide the plane into three regions, defined as follows:

$N_A > 1$, Region I,

$N_A < 1$, $N_D < 1$, Region II,

$N_D > 1$, Region III.

Arrays located in Region I are characterized as "collimated beam" arrays, which are wide enough that aperture effects of the beam cross section are important. These arrays may have small sidelobes. Region II arrays behave closely as described by Westervelt's theory[21] in the far field of the array, while Region III arrays are characterized by interactions in the far field of the primary waves, such that destructive interference reduces the efficiency of the nonlinear conversion process. No sidelobes are expected to be seen in Region II and Region III arrays. Table A1 summarizes the parameters of the arrays used in this experiment at $f_- = 250$ kHz. Also, $a^2/\lambda_0$ indicates the position of the outermost axial maximum for the mean primary frequency. The two arrays belong clearly to different parameter regions.

TABLE AI. Array parameters at $f_- = 250$ kHz in "lamp oil."

| Array | $L_A$ cm | $a^2/\lambda_0$ cm | $N_f$ | $N_F$ | $N_A$ | $N_D$ | Region |
|---|---|---|---|---|---|---|---|
| 4 MHz | 9.5 | 73 | 0.057 | 0.142 | 1.68 | 0.034 | I |
| 2 MHz | 45 | 21 | 0.132 | 0.567 | 0.64 | 0.21 | II |


[1] T. G. Muir, "A survey of several nonlinear acoustics experiments on travelling wavefields", in *Proceedings of the 1973 Symposium on Finite Amplitude Wave Effects in Fluids, Copenhagen*, edited by L. Bjørnø (I.P.C. Science and Technology, Guildford, 1974).

[2] T. G. Muir, C. W. Horton, Sr., and L. A. Thompson, "The penetration of highly directional acoustic beams into sediments," J. Sound Vib. **64**, 539–551 (1979).

[3] C. W. Horton, Sr., "The penetration of highly directional acoustic beams into a sediment bottom. Part I," Applied Research Laboratories Technical Report No. 74-28, Applied Research Laboratories, The University of Texas at Austin, Austin (1974).

[4] H. O. Berktay and A. H. A. Moustafa, "Transmission of a narrow beam of sound across a boundary between two fluids," in *Proceedings of the Nato Conference on Bottom-Interacting Ocean Acoustics*, SACLANT ASW Centre, Italy, 9–13 June 1980, edited by W. A. Kuperman and F. B. Jensen (Plenum, New York, 1980).

[5] J. Naze Tjøtta and S. Tjøtta, "Theoretical study of the penetration of highly directional acoustic beams into sediments," J. Acoust. Soc. Am. **69**, 998–1008 (1985).

[6] D. J. Wingham, "A theoretical study of the penetration of a water sediment interface by a parametric beam," J. Acoust. Soc. Am. **76**, 1192–1200 (1984).

[7] D. J. Wingham, N. G. Pace, and R. V. Ceen, "An experimental study of the penetration of a water–sediment interface by a parametric beam," J. Acoust. Soc. Am. **79**, 363–374 (1986).

[8] F. Jensen and H. Schmidt, "Subcritical penetration of narrow Gaussian beams into sediments," J. Acoust. Soc. Am. **82**, 574–579 (1987).

[9] H. Schmidt and F. Jensen, "A full wave solution for propagation in multilayered viscoelastic media with application to gaussian beam reflection at fluid–solid interfaces," J. Acoust. Soc. Am. **77**, 813–825 (1985).

[10] J. Naze Tjøtta, H. Sagen, and S. Tjøtta, "Interaction of a sound beam with a two fluid interface: Numerical results and asymptotic expressions," J. Acoust. Soc. Am. **85**, 24–38 (1989).

[11] H.-C. Salvesen, J. Naze Tjøtta and S. Tjøtta, "Transmission and reflection of a sound beam at a two-fluid interface: Simplified expressions for the beam displacement," in *Proceedings of the 13th International Congress on Acoustics*, edited by P. Pravica and G. Draculic (SAVA Center, Belgrade, Yugoslavia, 1989).

[12] K. L. Williams, L. J. Satkowiak, and D. R. Bugler: "Linear and parametric array transmission across a water–sand interface: Theory, experiment, and observation of beam displacement," J. Acoust. Soc. Am. **86**, 311–325 (1989).

[13] M. B. Moffet and R. H. Mellen, "Model for parametric acoustic sources," J. Acoust. Soc. Am. **61**, 325–337 (1977).

[14] H. Hobaek, "Parametric acoustic transmitting arrays," Scientific/Technical Rep. No. 99, Department of Physics, University of Bergen, 1977.

[15] M. Vestrheim and H. Hobaek, "Angular distribution of nonlinearly generated difference frequency sound", in *Proceedings of Symposium on Non-*

*linear Acoustics held at the University of Birmingham on 1st and 2nd April 1971* (The British Acoustical Society, London, 1972) pp. 159–169.
[16] H. Hobaek and S. Tjøtta, "Theory of parametric acoustic arrays," J. Phys. **40**, C8, 101–110 (1979).
[17] G. Saracco, "Transmission acoustique à travers le dioptre air-eau," J. Acoustique **1**, 71–80 (1988).
[18] L. M. Brekhovskikh, *Waves in Layered Media* (Academic, New York, 1980).
[19] J. Naze Tjøtta and S. Tjøtta, "Interaction of sound waves. Part III: Two real beams," J. Acoust. Soc. Am. **83**, 487–495 (1988).
[20] M. Vestrheim, "A parameter representation of the parametric array," in *Proceedings of the 1973 Symposium on Finite Amplitude Wave Effects in Fluids*, Copenhagen, edited by L. Bjørnø (I.P.C. Science and Technology, Guildford, 1974).
[21] P. J. Westervelt, "Parametric acoustic array," J. Acoust. Soc. Am. **35**, 535–537 (1963).